

# Dynamic twisting and imaging of moiré crystals

Qixuan Zhang,<sup>1</sup> Trevor Senaha,<sup>2</sup> Ruolun Zhang,<sup>2</sup> Chen Wu,<sup>2</sup> Lingyuan Lyu,<sup>2</sup> Leonard W. Cao,<sup>2</sup>  
Jason Tresback,<sup>3</sup> Andrew Dai,<sup>2</sup> Kenji Watanabe,<sup>4</sup> Takashi Taniguchi,<sup>4</sup> and Monica T. Allen<sup>2</sup>

<sup>1</sup>Program in Material Science and Engineering, University of California, San Diego, CA 92093, USA

<sup>2</sup>Department of Physics, University of California, San Diego, CA 92093, USA

<sup>3</sup>Center for Nanoscale Systems, Harvard University, Cambridge, MA 02138, USA

<sup>4</sup>National Institute for Materials Science, Namiki 1-1, Tsukuba, Ibaraki 305-0044, Japan

(Dated: July 17, 2023)

The electronic band structure is an intrinsic property of solid-state materials that is intimately connected to the crystalline arrangement of atoms. Moiré crystals, which emerge in twisted stacks of atomic layers, feature a band structure that can be continuously tuned by changing the twist angle between adjacent layers [1–4]. This class of artificial materials blends the discrete nature of the moiré superlattice with intrinsic symmetries of the constituent materials, providing a versatile platform for investigation of correlated phenomena whose origins are rooted in the geometry of the superlattice, from insulating states at “magic angles” [5–8] to flat bands in quasicrystals [9]. Here we present a route to mechanically tune the twist angle of individual atomic layers with a precision of a fraction of a degree inside a scanning probe microscope, which enables continuous control of the electronic band structure *in situ*. Using nanostructured rotor devices, we achieve the collective rotation of a single layer of atoms with minimal deformation of the crystalline lattice. In twisted bilayer graphene, we demonstrate nanoscale control of the moiré superlattice periodicity via external rotations, as revealed using piezoresponse force microscopy [10]. We also extend this methodology to create twistable boron nitride devices, which could enable dynamic control of the domain structure of moiré ferroelectrics [11–13]. This approach provides a route for real-time manipulation of moiré materials, allowing for systematic exploration of the phase diagrams at multiple twist angles in a single device.

In conventional solid-state materials, the band structure is a fixed property determined by the composition and arrangement of atoms in a crystalline lattice. Many recent breakthroughs have been enabled by synthesis of crystals with novel band structures, ranging from the development of flat band materials that host correlated phases to the discovery of quantum-relativistic crystals whose low energy electronic band structures give rise to charges that mimic relativistic particles [14, 15]. A contrasting “bottom-up” approach is the realization of artificial quantum matter using platforms such as ultracold atoms and trapped ions, which benefit from exquisite control and tunability [16–18]. However, the weakness of many-body interactions in these artificial systems has hampered investigation of certain classes of correlated states, while access to low temperature regimes has proven challenging. Two-dimensional moiré materials merge the best of both approaches by pairing strong correlations (and access to non-trivial band topology) with the tunability afforded by twisted heterostructures, for example enabling simulation of the Hub-

bard model in triangular superlattices [1–4, 19–22].

Twisted moiré superlattices – consisting of two atomic crystals rotated by an angle – exhibit behavior that departs dramatically from that of the constituent monolayers and form a highly tunable platform for exploration of emergent phenomena driven by interactions. Such artificially layered systems can be created in the lab by isolating single atomic layers from a bulk crystal and stacking them in a precise configuration using micromanipulators, a technique known as “van der Waals epitaxy” [23–25]. The moiré interference pattern features a modulation of the relative alignment between sublattice atoms, thus yielding spatial variations in the tunneling amplitude and interlayer potential difference across the superlattice. At small rotations that yield flat bands, electronic interactions dominate over the kinetic energy, giving rise to a rich phase diagram that can be tuned with twist angle [2, 5, 26, 27]. For example, twisted bilayer graphene exhibits a constellation of correlated states at a “magic angle” of  $1.1^\circ$ , including superconductivity, Mott insulators, and a quantum anomalous Hall effect [2, 7, 8]. In semiconductor Group IV transition metal dichalcogenides (TMDs), a richer picture emerges because broken inversion symmetry and spin-orbit coupling lift the spin degeneracy in the  $\pm K$  valence bands, which can lead to the formation of many-body topological phases in twisted heterostructures [22, 27–29].

The periodic structure of the superlattice can also be leveraged for a broad range of practical applications, from the creation of photonic crystals for nano-light [30] to tunable angle-dependent platforms for electrochemistry [31]. However, existing methods for the construction of moiré heterostructures lock the atomic arrangement of the superlattice in place after device fabrication, so investigation of multiple twist angles requires measurements of ensembles of devices with different disorder profiles, strain, electrostatic environments. This motivates our development of a new technology to dynamically rotate individual layers of an active device structure, which should allow for continuous investigation of phase diagrams as a function of angle in a highly controlled setting.

In this work, we present a method for real-time rotation of individual atomic layers with a precision of a fraction of a degree, which should enable unprecedented control over the topology of the band structure and electronic interactions in moiré superlattices. We demonstrate manipulation of the superlattice periodicity with nanoscale resolution in response to this angular rotation, achieved through direct imaging of the moiré superlattice using piezoresponse force microscopy (PFM) [10]. Furthermore, the proposed nanomechanical ap-

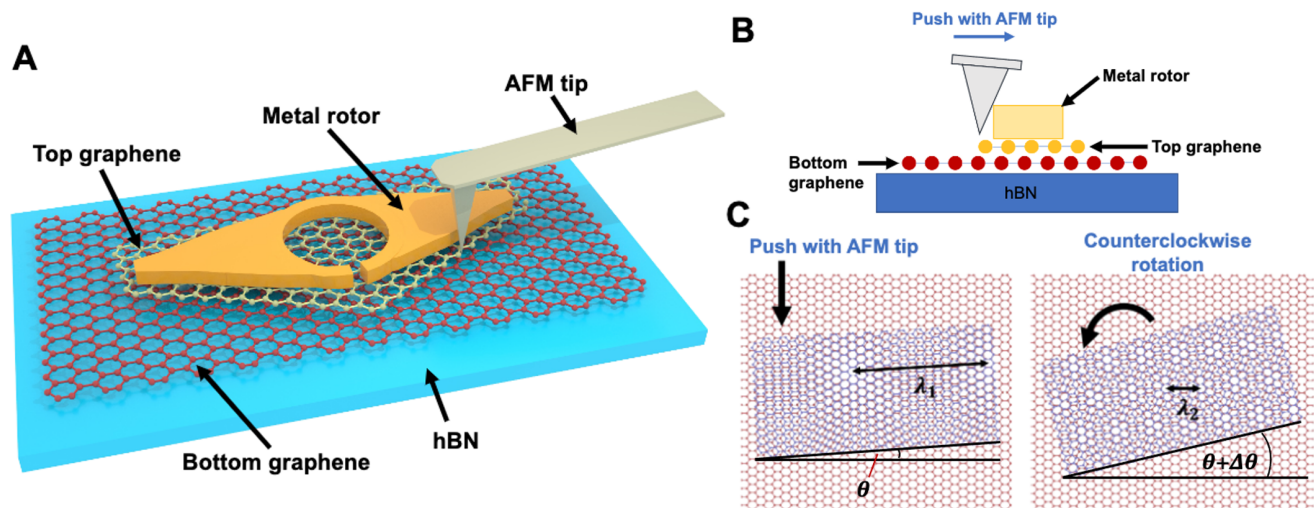


FIG. 1. **Real-time mechanical manipulation of a moiré superlattice, enabling *in situ* control over the twist angle.** (A) Schematic illustration of a twisted bilayer graphene rotor device and dynamic manipulation of the twist angle using a scanning probe tip. The circular opening in the middle of the rotor frame provides space for high resolution imaging and measurements of the moiré superlattice. (B) Cross-sectional view of the tip-induced mechanical manipulation of the rotor frame during a contact-mode AFM line scan. (C) Schematic of the bilayer graphene moiré superlattice in the rotor device before (*left panel*) and after (*right panel*) the twisting process, revealing the change in the moiré unit cell size  $\lambda_1 \rightarrow \lambda_2$  due to the change in the twist angle  $\theta \rightarrow \theta + \Delta\theta$ .

proach offers a precise method of tuning the device to targeted angles that may host interesting phenomena, such as “magic angles” in twisted bilayer graphene or specific angles that host topological insulator states [2, 7, 8, 22, 27–29].

A schematic illustration of the rotor geometry and manipulation methodology is presented in Figure 1. We employ mechanical exfoliation and standard dry transfer methods to assemble twisted bilayer graphene and twisted double-layer hexagonal boron nitride (hBN) heterostructures, which are deposited onto a thicker hBN base layer [25]. As shown in Fig. 1 A, a nanostructured metal rotor is patterned on the top monolayer of the twisted heterostructure, allowing it to rotate freely with respect to the bottom flake. The rotor frame provides structural support that enables rigid rotation of the entire top atomic layer, minimizing the likelihood of stretching or tearing during the mechanical manipulation process. The rotors are patterned with electron beam (e-beam) lithography, followed by e-beam evaporation of 15 nm Cr / 100 nm Au (Fig. S1 in the Supplementary Information). The rotor is designed to cover most of the exposed area of the top monolayer, which allows the entire flake to move freely without being pinned onto the lower layer.

A Park NX20 scanning probe microscope with combined atomic force microscopy (AFM) and piezoresponse force microscopy (PFM) capabilities is used to both image and manipulate the twisted heterostructures *in situ*. As demonstrated in prior work, an AFM cantilever probe can be used to controllably apply lateral forces and move nanostructures (including multilayer hBN and graphite flakes) on a flat surface [32–39]. Our *in situ* rotation process for twisted bilayer graphene is conceptually illustrated in Fig.1 B. When the moving AFM probe comes into contact with the metal rotor, it will exert a

horizontal force on the structure. The adhesive force between the gold rotor frame and the top flake is considerably larger than the inter-layer friction and van der Waals forces between the graphene layers; therefore, the rotor-supported top flake will rigidly rotate on the surface of the bottom flake once the force exerted by the AFM probe exceeds the static friction limit between the two layers. Thus, the rotation process can be precisely controlled by programming the trace of the contact-mode AFM line scans. The rotation of the top layer with respect to the lower layer directly changes the moiré periodicity, as illustrated in Fig. 1 C.

This *in situ* manipulation procedure allows for highly controlled translational and rotational inter-layer movement in twisted heterostructures, as shown in Fig. 2. The first step involves acquisition of a tapping-mode AFM image encompassing the entire metal frame and the surrounding area, which serves as a reference for later manipulation steps (Fig. 2 A, D). To obtain precise information on the initial orientation of the metal frame, high resolution AFM scans of the targeted pushing point on the lever arm are also obtained (Fig. S2 in the Supplementary Information). The manipulation process is performed with the AFM tip in contact mode, and the scanning direction of the tip should be oriented perpendicular to the lever arm of the rotor. The white arrow in Fig. 2 A indicates the point of contact between the scanning tip and the rotor, and the resulting direction of the induced rotation is shown in Fig. 2 B. When the AFM tip is scanned from the substrate towards the lever arm, the tip will push on the side wall of the rotor and a large longitudinal force exceeding 500 nN is applied to the metal frame. (The forces required to achieve *in situ* twisting of double-layer graphene typically fall within the range of 600 nN to 1400 nN.) Note that the contact-mode

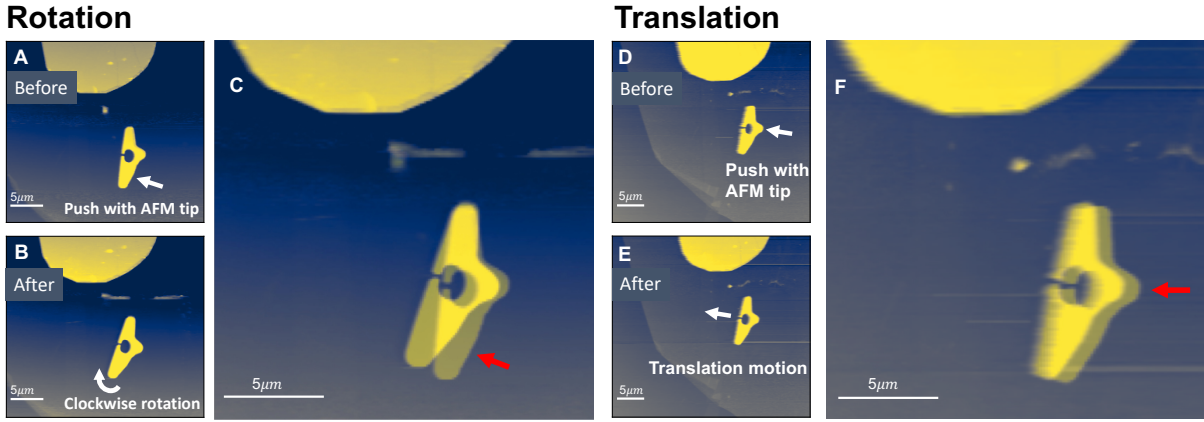


FIG. 2. **Dynamic rotation and translation of twisted bilayer graphene driven by an atomic force microscope.** (A) and (B) Tapping-mode AFM image of rotor device I before and after rotation, respectively. The rotor frame is lithographically patterned on a twisted bilayer graphene heterostructure, allowing the upper monolayer to rotate freely with respect to the lower layer. Because the rotor is several hundred times thicker than a graphene monolayer, the large height contrast makes the graphene flake almost invisible. (C) A superimposed image of panels (A) and (B) reveals the clockwise twisting of the rotor induced by *in situ* manipulation. The red arrow indicates the direction of the horizontal force applied by the AFM probe. (D) and (E) Tapping-mode AFM image of rotor device I before and after translation, respectively. (F) A superimposed image of panels (D) and (E) reveals the lateral translation of the upper graphene monolayer with respect to the lower layer.

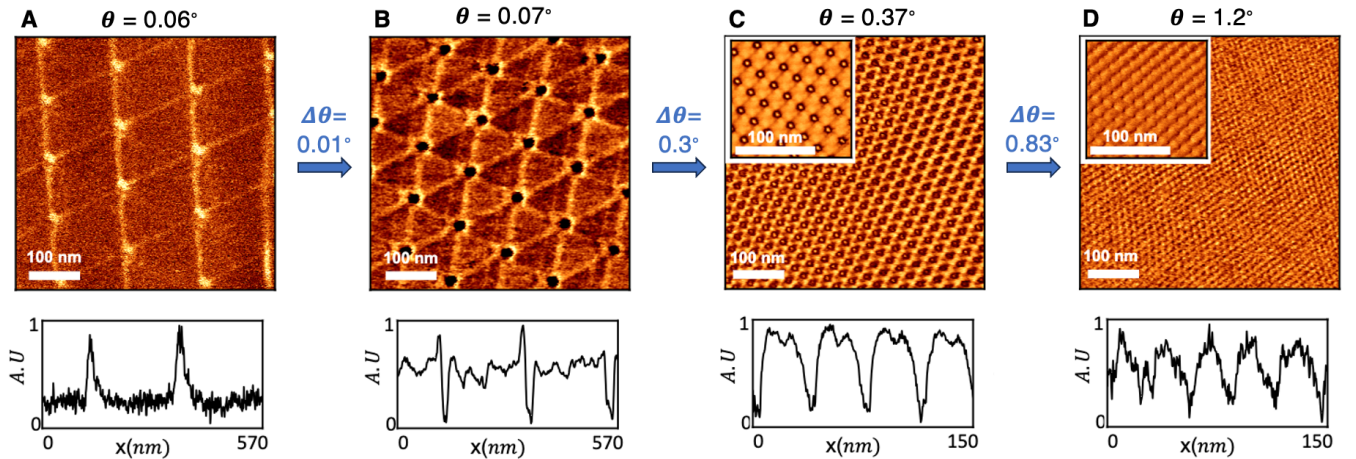


FIG. 3. **Nanoscale tunability of the moiré superlattice geometry, achieved via *in situ* rotation of twisted bilayer graphene.** (A) Image of the moiré superlattice that forms at a twist angle of  $\theta = 0.06^\circ$ , obtained using piezoresponse force microscopy (PFM). *Lower panel:* Cross-sectional line cut that shows modulations in the PFM signal associated with the superlattice. (B) After a tip-driven rotation of this twisted bilayer graphene device, which introduces a twist angle change of  $\Delta\theta = 0.01^\circ$ , a modified moiré superlattice with a smaller period emerges at the new twist angle of  $\theta + \Delta\theta = 0.07^\circ$ . Both the *in situ* rotation and PFM imaging are performed within the same microscope. (C) and (D) PFM images of the moiré superlattice in the same rotor device after additional rotations, revealing the real-space evolution of the superlattice geometry that is induced by each successive rotation of the twist angle. (C) and (D) show the moiré patterns at  $\theta = 0.37^\circ$  and  $\theta = 1.2^\circ$ , respectively. The insets are higher resolution  $150\text{ nm} \times 150\text{ nm}$  PFM scans.

scan window should be defined to have a high aspect ratio or even be set to a single line scan, which pinpoints the specific location of the point of contact between the tip and rotor. The rotation angle can be tuned by changing the distance pushed by the AFM tip and the location of the point of contact on the rotor. Once the manipulation step is completed, another tapping-mode AFM image of the entire rotor frame and the surrounding area is obtained to quantify the induced rotation (Fig. 2B). To track the change in orientation of the rotor, Fig. 2C plots the “before” and “after” images superimposed on

top of each other. By comparing the two images, it is possible to resolve the twisting of the heterostructure (see Fig. S3 in the Supplementary Information). To more accurately identify the twist angle of the bilayer before and after the manipulation, PFM can be used to image the moiré pattern and extract its periodicity.

Fig. 2 D-F shows the second type of manipulation: lateral translation of the rotor. While tip-controlled manipulation can be used to induce both rotation and translation, their relative proportions can be controlled by adjusting the po-

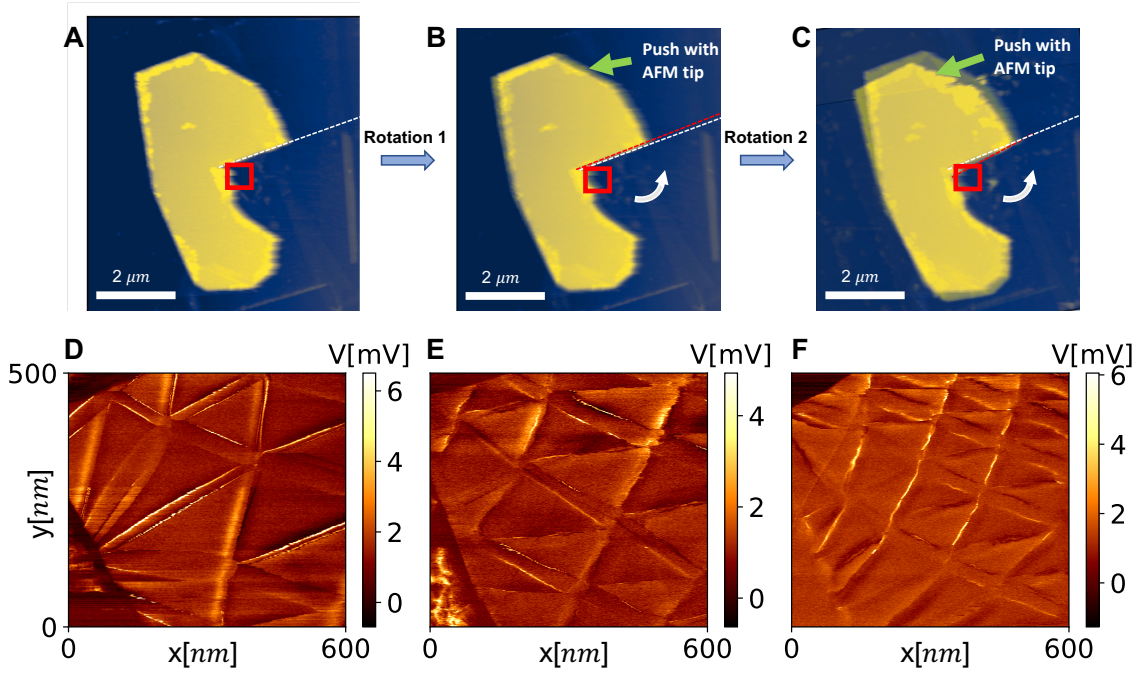


FIG. 4. **Tuning the ferroelectric domain structure of twisted double-layer hBN.** (A-C) A sequence of AFM images of an hBN rotor device before and after two successive rotations driven by the scanning probe tip. The white and red dashed lines mark the initial and final orientations of rotor, respectively. The green arrows in (B) and (C) indicate the push point location and direction of the applied in-plane force, while the red squares mark the locations of the PFM imaging windows. (D-F) Sequence of PFM images showing the evolution of the moiré domain structure in the twisted double-layer hBN induced by the mechanical rotation process. The imaging and *in situ* manipulation steps were performed within the same microscope.

sition of the push point. Nearly pure translation could be achieved by aligning the tip contact point with the center of mass of the metal rotor structure. The sliding resistance between the two graphene sheets arises mainly from interlayer friction and resistive forces caused by uneven topography and organic residues from nanofabrication. We find that contact-mode cleaning, a standard technique for improving the surface cleanliness of van der Waals heterostructures[40, 41], effectively reduces the sliding resistance between two layers by removing organic residues from the e-beam lithography process. Additionally, heating the sample stage decreases the interlayer friction, which facilitates the nanomechanical manipulation process.

The main goal of this manipulation technique is to exert precise, controllable changes to the structure and unit cell size of a moiré crystal. In Fig. 3, we demonstrate dynamic rotation of a single monolayer within a twisted bilayer graphene heterostructure and observe a series of controlled changes in the superlattice period. During the rotation process, the device was tuned to four distinct twist angles:  $0.06^\circ$ ,  $0.07^\circ$ ,  $0.37^\circ$ , and  $1.20^\circ$ . The sequence of PFM images in Fig.3A-D show the evolution of the moiré pattern with twist angle; all scans were captured from the same location on the heterostructure. These images reveal nearly isotropic changes in the period of the superlattice for each successive twist angle change  $\Delta\theta$ . The twist angle  $\theta$  for each configuration can be extracted experimentally from the measured superlattice pe-

riod, as discussed in the Supplementary Information. From the PFM data, we observe no obvious stretching or deformation introduced to the superlattice during the rotation process. This is one difference between the proposed approach and other methods for mechanical manipulation of van der Waals heterostructures, which can simultaneously introduce strain in the process. To show reproducibility, we also demonstrate the twisting-induced manipulation of the moiré superlattice in a separate twisted bilayer graphene device, which exhibits similar behavior (see Fig.S6 in the Supplementary Information).

To achieve the sequence of rotations featured in Fig.3A-D, the sample stage was heated up to  $190^\circ\text{C}$  to lower the interlayer friction between the graphene flakes, and the longitudinal forces used in the AFM manipulation process ranged from 1000 nN to 1500 nN. The smallest twist angle change that we could demonstrate experimentally is roughly  $\Delta\theta = 0.01^\circ$ , as illustrated in Fig. 3A-B, which was achieved by inducing a 30 nm displacement of the rotor arm. The differences between the expected rotation angle ( $\Delta\alpha = 0.012^\circ$ , estimated based on the lateral displacement of the lever arm) and the actual twist angle change ( $\Delta\theta = 0.01^\circ$ , extracted experimentally from the measured superlattice period) can be attributed to the natural scale errors in the AFM scanning program and the lateral deflection of the tip during the pushing process, which adds a small offset to the tip travel distance (see Supplementary Information for details). AFM images of the rotor device used for these measurements are provided in Supplementary Figs.

S4-S5.

In order to demonstrate the broader applicability of this method for other classes of 2D materials, we extend this technique to twisted double-layer hBN, which for example could enable *in situ* tuning of the ferroelectric domain structure by changing the twist angle [11–13]. The fabrication procedure and heterostructure geometry are conceptually similar that illustrated schematically in Fig. 1A (see Fig. 4 and Fig. S1 in the Supplementary Information). Fig. 4A-C show tapping-mode AFM images of the rotor configurations prior to manipulation, after the first rotation, and after the second rotation, respectively. By manipulating the rotor, we are able to induce corresponding changes in the moiré domain structure, as revealed in the PFM images displayed in Fig. 4 D-F. The longitudinal forces required to manipulate hBN rotors, which fall in the range of 600 nN to 1200 nN, are typically smaller than those required to rotate twisted bilayer graphene.

**Conclusion and Outlook.** In contrast to many existing state-of-the-art twisted bilayer heterostructures, in which the atoms are locked into a specific configuration after fabrication, the devices presented here offer a new route to dynamically tune and image moiré superlattices. This is achieved via controlled rotation of a single atomic layer with respect to another, which can be performed *in situ* within a microscope. The high level of angular control provides access to multiple twist angles and superlattice configurations, which enables systematic investigation of a wide variety of phenom-

ena within a single device. This method can also be extended to monolayer van der Waals materials beyond graphene, opening the door to dynamic control over the ferroelectric domain structure in angle-aligned hBN and TMDs [42], or manipulation of the periodicity of topological spin textures in moiré magnets [43].

The twisted heterostructure remains exposed throughout the entire rotation process to allow for easy interrogation with optical or scanning probes, which could be useful for a broad range of experiments across many scientific disciplines. The *in situ* twisting technique presented here does not require any specialized scanning probe microscopy instrumentation to perform; it can be implemented using a commercial AFM and nanofabrication equipment available in a standard cleanroom. We hope that this accessibility will allow for broad adoption of this methodology across the community.

## ACKNOWLEDGEMENTS

We gratefully acknowledge funding support from the UC Office of the President, specifically the UC Laboratory Fees Research Program (award LFR-20-653926) and the AFOSR Young Investigator Program (award FA9550-20-1-0035). This work was performed, in part, at the San Diego Nanotechnology Infrastructure (SDNI) of UCSD, a member of the National Nanotechnology Coordinated Infrastructure, which is supported by the National Science Foundation (Grant ECCS-2025752).

- 
- [1] Guohong Li, A Luican, JMB Lopes dos Santos, AH Castro Neto, A Reina, J Kong, and EY Andrei, “Observation of van Hove singularities in twisted graphene layers,” *Nature physics* **6**, 109–113 (2010).
- [2] Rafi Bistritzer and Allan H MacDonald, “Moiré bands in twisted double-layer graphene,” *Proceedings of the National Academy of Sciences* **108**, 12233–12237 (2011).
- [3] Matthew Yankowitz, Jiamin Xue, Daniel Cormode, Javier D Sanchez-Yamagishi, K Watanabe, T Taniguchi, Pablo Jarillo-Herrero, Philippe Jacquod, and Brian J LeRoy, “Emergence of superlattice dirac points in graphene on hexagonal boron nitride,” *Nature physics* **8**, 382–386 (2012).
- [4] Stephen Carr, Daniel Massatt, Shiang Fang, Paul Cazeaux, Mitchell Luskin, and Efthimios Kaxiras, “Twistronics: Manipulating the electronic properties of two-dimensional layered structures through their twist angle,” *Physical Review B* **95**, 075420 (2017).
- [5] Kyoungwan Kim, Ashley DaSilva, Shengqiang Huang, Babak Fallahzad, Stefano Larentis, Takashi Taniguchi, Kenji Watanabe, Brian J LeRoy, Allan H MacDonald, and Emanuel Tutuc, “Tunable moiré bands and strong correlations in small-twist-angle bilayer graphene,” *Proceedings of the National Academy of Sciences* **114**, 3364–3369 (2017).
- [6] VI Iglovikov, F Hébert, B Grémaud, GG Batrouni, and RT Scalettar, “Superconducting transitions in flat-band systems,” *Physical Review B* **90**, 094506 (2014).
- [7] Yuan Cao, Valla Fatemi, Ahmet Demir, Shiang Fang, Spencer L Tomarken, Jason Y Luo, Javier D Sanchez-Yamagishi, Kenji Watanabe, Takashi Taniguchi, Efthimios Kaxiras, *et al.*, “Correlated insulator behaviour at half-filling in magic-angle graphene superlattices,” *Nature* **556**, 80–84 (2018).
- [8] Yuan Cao, Valla Fatemi, Shiang Fang, Kenji Watanabe, Takashi Taniguchi, Efthimios Kaxiras, and Pablo Jarillo-Herrero, “Unconventional superconductivity in magic-angle graphene superlattices,” *Nature* **556**, 43–50 (2018).
- [9] Pilkyung Moon, Mikito Koshino, and Young-Woo Son, “Quasicrystalline electronic states in 30° rotated twisted bilayer graphene,” *Physical Review B* **99**, 165430 (2019).
- [10] Leo J McGilly, Alexander Kerelsky, Nathan R Finney, Konstantin Shapovalov, En-Min Shih, Augusto Ghiotto, Yihang Zeng, Samuel L Moore, Wenjing Wu, Yusong Bai, *et al.*, “Visualization of moiré superlattices,” *Nature Nanotechnology* **15**, 580–584 (2020).
- [11] Zhiren Zheng, Qiong Ma, Zhen Bi, Sergio de La Barrera, Ming-Hao Liu, Nannan Mao, Yang Zhang, Natasha Kiper, Kenji Watanabe, Takashi Taniguchi, *et al.*, “Unconventional ferroelectricity in moiré heterostructures,” *Nature* **588**, 71–76 (2020).
- [12] CR Woods, P Ares, H Nevison-Andrews, MJ Holwill, R Fabregas, Francisco Guinea, AK Geim, KS Novoselov, NR Walet, and L Fumagalli, “Charge-polarized interfacial superlattices in marginally twisted hexagonal boron nitride,” *Nature communications* **12**, 347 (2021).
- [13] Kenji Yasuda, Xirui Wang, Kenji Watanabe, Takashi Taniguchi, and Pablo Jarillo-Herrero, “Stacking-engineered ferroelectricity in bilayer boron nitride,” *Science* **372**, 1458–1462 (2021).

- [14] Tim O Wehling, Annica M Black-Schaffer, and Alexander V Balatsky, “Dirac materials,” *Advances in Physics* **63**, 1–76 (2014).
- [15] Oleg Derzhko, Johannes Richter, and Mykola Maksymenko, “Strongly correlated flat-band systems: The route from heisenberg spins to hubbard electrons,” *International Journal of Modern Physics B* **29**, 1530007 (2015).
- [16] Nathan Goldman, Jan C Budich, and Peter Zoller, “Topological quantum matter with ultracold gases in optical lattices,” *Nature Physics* **12**, 639–645 (2016).
- [17] Ian B Spielman, Nathan Goldman, Indubala I Satija, Predrag Nikolic, Alejandro Bermudez, Miguel A Martin-Delgado, and Maciej Lewenstein, “Engineering time-reversal invariant topological insulators with ultra-cold atoms,” (2010).
- [18] Ian B Spielman, William D Phillips, and James V Porto, “Mott-insulator transition in a two-dimensional atomic bose gas,” *Physical Review Letters* **98**, 080404 (2007).
- [19] Hubbard, “Electron correlations in narrow energy bands,” *Proceedings of the Royal Society of London. Series A. Mathematical and Physical Sciences* **281**, 401–419 (1963).
- [20] Yanhao Tang, Lizhong Li, Tingxin Li, Yang Xu, Song Liu, Katayun Barmak, Kenji Watanabe, Takashi Taniguchi, Allan H MacDonald, Jie Shan, *et al.*, “Simulation of hubbard model physics in wse<sub>2</sub>/ws<sub>2</sub> moiré superlattices,” *Nature* **579**, 353–358 (2020).
- [21] Kin Fai Mak and Jie Shan, “Semiconductor moiré materials,” *Nature Nanotechnology* **17**, 686–695 (2022).
- [22] Haining Pan, Fengcheng Wu, and Sankar Das Sarma, “Quantum phase diagram of a moiré-hubbard model,” *Physical Review B* **102**, 201104 (2020).
- [23] Kostya S Novoselov, Andre K Geim, Sergei V Morozov, Deng Jiang, Yanshui Zhang, Sergey V Dubonos, Irina V Grigorieva, and Alexandr A Firsov, “Electric field effect in atomically thin carbon films,” *science* **306**, 666–669 (2004).
- [24] Andre K Geim and Irina V Grigorieva, “Van der waals heterostructures,” *Nature* **499**, 419–425 (2013).
- [25] Cory R Dean, Andrea F Young, Inanc Meric, Chris Lee, Lei Wang, Sebastian Sorgenfrei, Kenji Watanabe, Takashi Taniguchi, Phillip Kim, Kenneth L Shepard, *et al.*, “Boron nitride substrates for high-quality graphene electronics,” *Nature nanotechnology* **5**, 722–726 (2010).
- [26] Matthew Yankowitz, Shaowen Chen, Hryhorii Polshyn, Yuxuan Zhang, K Watanabe, T Taniguchi, David Graf, Andrea F Young, and Cory R Dean, “Tuning superconductivity in twisted bilayer graphene,” *Science* **363**, 1059–1064 (2019).
- [27] Fengcheng Wu, Timothy Lovorn, Emanuel Tutuc, Ivar Martin, and AH MacDonald, “Topological insulators in twisted transition metal dichalcogenide homobilayers,” *Physical review letters* **122**, 086402 (2019).
- [28] Yihang Zeng, Zhengchao Xia, Kaifei Kang, Jiacheng Zhu, Patrick Knüppel, Chirag Vaswani, Kenji Watanabe, Takashi Taniguchi, Kin Fai Mak, and Jie Shan, “Integer and fractional chern insulators in twisted bilayer mote<sub>2</sub>,” *arXiv preprint arXiv:2305.00973* (2023).
- [29] Jiaqi Cai, Eric Anderson, Chong Wang, Xiaowei Zhang, Xiaoyu Liu, William Holtzmann, Yinong Zhang, Fengren Fan, Takashi Taniguchi, Kenji Watanabe, *et al.*, “Signatures of fractional quantum anomalous hall states in twisted mote<sub>2</sub> bilayer,” *arXiv preprint arXiv:2304.08470* (2023).
- [30] SS Sunku, GuangXin Ni, Bor-Yuan Jiang, Hyobin Yoo, Aaron Sternbach, AS McLeod, T Stauber, Lin Xiong, Takashi Taniguchi, Kenji Watanabe, *et al.*, “Photonic crystals for nano-light in moiré graphene superlattices,” *Science* **362**, 1153–1156 (2018).
- [31] Yun Yu, Kaidi Zhang, Holden Parks, Mohammad Babar, Stephen Carr, Isaac M Craig, Madeline Van Winkle, Artur Lyssenko, Takashi Taniguchi, Kenji Watanabe, *et al.*, “Tunable angle-dependent electrochemistry at twisted bilayer graphene with moiré flat bands,” *Nature Chemistry* **14**, 267–273 (2022).
- [32] Elad Koren, Itai Leven, Emanuel Lörtcher, Armin Knoll, Oded Hod, and Urs Duerig, “Coherent commensurate electronic states at the interface between misoriented graphene layers,” *Nature nanotechnology* **11**, 752–757 (2016).
- [33] Tarun Chari, Rebeca Ribeiro-Palau, Cory R Dean, and Kenneth Shepard, “Resistivity of rotated graphite–graphene contacts,” *Nano letters* **16**, 4477–4482 (2016).
- [34] Rebeca Ribeiro-Palau, Changjian Zhang, Kenji Watanabe, Takashi Taniguchi, James Hone, and Cory R Dean, “Twistable electronics with dynamically rotatable heterostructures,” *Science* **361**, 690–693 (2018).
- [35] Cheng Hu, Tongyao Wu, Xinyue Huang, Yulong Dong, Jiajun Chen, Zhichun Zhang, Bosai Lyu, Saiqun Ma, Kenji Watanabe, Takashi Taniguchi, *et al.*, “In-situ twistable bilayer graphene,” *Scientific Reports* **12**, 204 (2022).
- [36] Mäelle Kapfer, Bjarke S Jessen, Megan E Eisele, Matthew Fu, Dorte R Danielsen, Thomas P Darlington, Samuel L Moore, Nathan R Finney, Ariane Marchese, Valerie Hsieh, *et al.*, “Programming moiré patterns in 2d materials by bending,” *arXiv preprint arXiv:2209.10696* (2022).
- [37] Andrew Z Barabas, Ian Sequeira, Yuhui Yang, Aaron H Barajas-Aguilar, Takashi Taniguchi, Kenji Watanabe, and Javier D Sanchez-Yamagishi, “Mechanically reconfigurable van der waals devices via low-friction gold sliding,” *Science Advances* **9**, eadf9558 (2023).
- [38] Yaping Yang, Jidong Li, Jun Yin, Shuigang Xu, Ciaran Mullan, Takashi Taniguchi, Kenji Watanabe, Andre K. Geim, Konstantin S. Novoselov, and Artem Mishchenko, “In situ manipulation of van der waals heterostructures for twistronics,” *Science Advances* **6**, eabd3655 (2020).
- [39] A. Inbar, J. Birkbeck, J. Xiao, T. Taniguchi, K. Watanabe, B. Yan, Y. Oreg, Ady Stern, E. Berg, and S. Ilani, “The quantum twisting microscope,” *Nature* **614**, 682–687 (2023).
- [40] AM Goossens, VE Calado, A Barreiro, K Watanabe, T Taniguchi, and LMK Vandersypen, “Mechanical cleaning of graphene,” *Applied Physics Letters* **100** (2012).
- [41] Niclas Lindvall, Alexey Kalabukhov, and August Yurgens, “Cleaning graphene using atomic force microscope,” *Journal of Applied Physics* **111** (2012).
- [42] Xirui Wang, Kenji Yasuda, Yang Zhang, Song Liu, Kenji Watanabe, Takashi Taniguchi, James Hone, Liang Fu, and Pablo Jarillo-Herrero, “Interfacial ferroelectricity in rhombohedral-stacked bilayer transition metal dichalcogenides,” *Nature nanotechnology* **17**, 367–371 (2022).
- [43] Hongchao Xie, Xiangpeng Luo, Zhipeng Ye, Zeliang Sun, Gaihua Ye, Suk Hyun Sung, Haiwen Ge, Shaohua Yan, Yang Fu, Shangjie Tian, *et al.*, “Evidence of non-collinear spin texture in magnetic moiré superlattices,” *Nature Physics* , 1–6 (2023).

## Supplementary Information

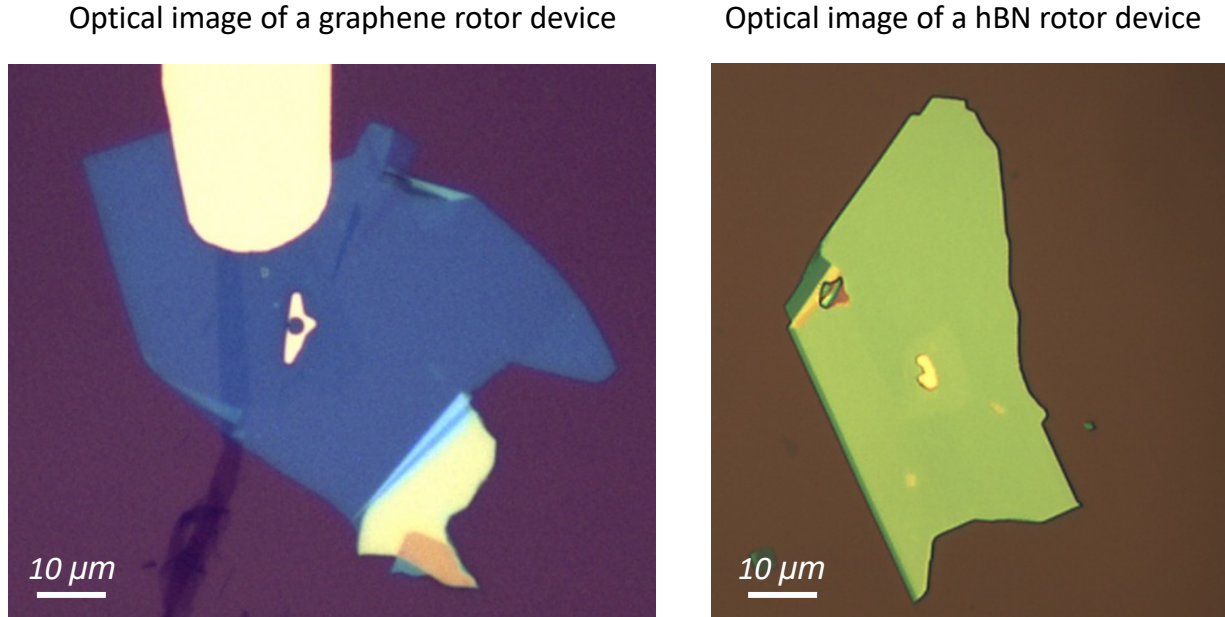


FIG. S1. Optical microscope images of the twisted bilayer graphene rotor featured in Fig.S6 (*left panel*) and the double-layer hBN rotor featured in Fig.4 (*right panel*). The nanopatterned rotor devices are defined using electron beam lithography, followed by deposition of 15nm Cr / 100nm Au using electron beam evaporation. The hBN and graphene flakes used in these devices are mechanically exfoliated from bulk crystals, and heterostructures are assembled using standard dry flake transfer methods.

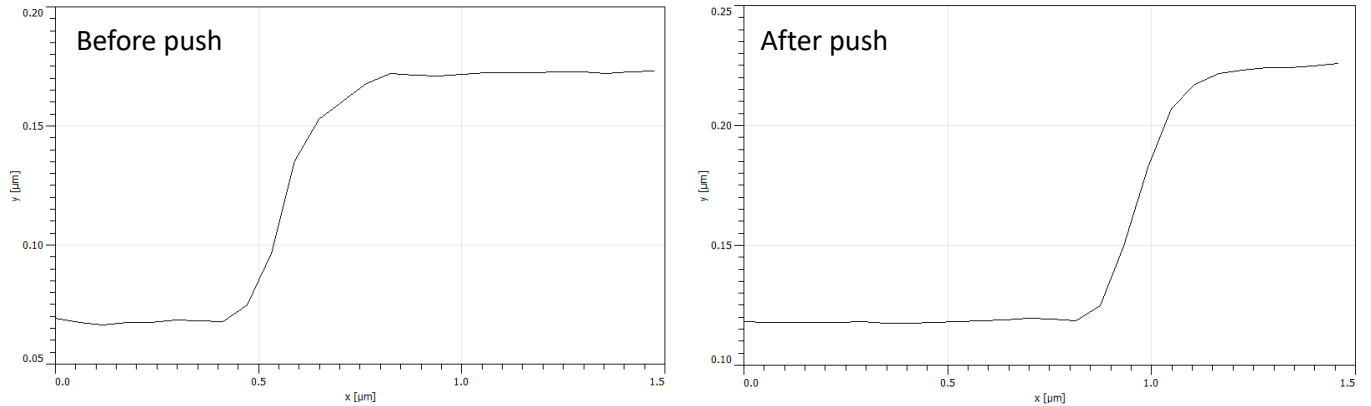


FIG. S2. Example tapping-mode AFM scans of the rotor edge before and after the tip-driven manipulation step. Before and after the pushing process, pairs of 1D line scans obtained in the same position are used to confirm the displacement of the rotor.

The estimated rotation angle ( $\Delta\alpha$ ) extracted from the tapping-mode AFM images is calculated based on the push distance of the rotor and rotation radius. The pushing distance can be extracted from the 1D line scan curve before and after the push (Fig. S2), while the rotation radius is determined from superimposed tapping-mode AFM images (Fig. 2; Fig. S3). The push distance can be finely controlled by pausing the tip in the middle of the contact mode line scan. The rotation radius is determined by drawing extension lines along one straight edge of the rotor before and after the rotation; the cross point can be considered as the rotation center.

The actual twist angles extracted from the measured moiré patterns are calculated using the following equation:

$$\theta = 2 \arcsin \frac{a}{2\lambda}$$

where  $\lambda$  is the moiré periodicity,  $a$  is the lattice constant, and  $\theta$  is the twist angle. For a graphene lattice,  $a = 0.246$  nm. The moiré periodicity  $\lambda$  can be determined experimentally from the piezoresponse force microscopy images (Fig. 3; Fig. S6).

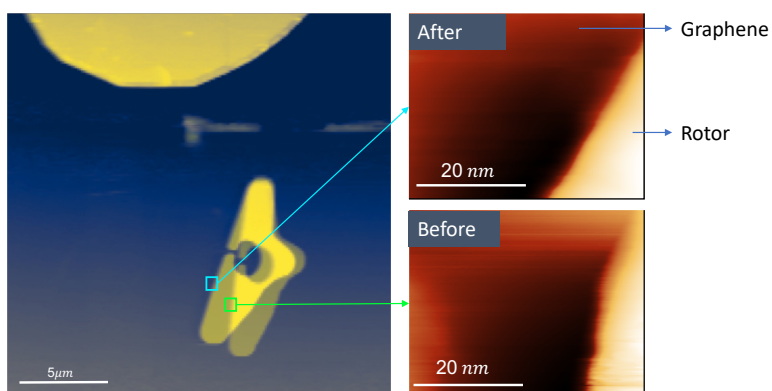


FIG. S3. Superimposed AFM images of the rotor device from Fig. 2 before and after rotation. In the two smaller panels on the right, the brightest feature on the right side is the edge of the rotor frame.

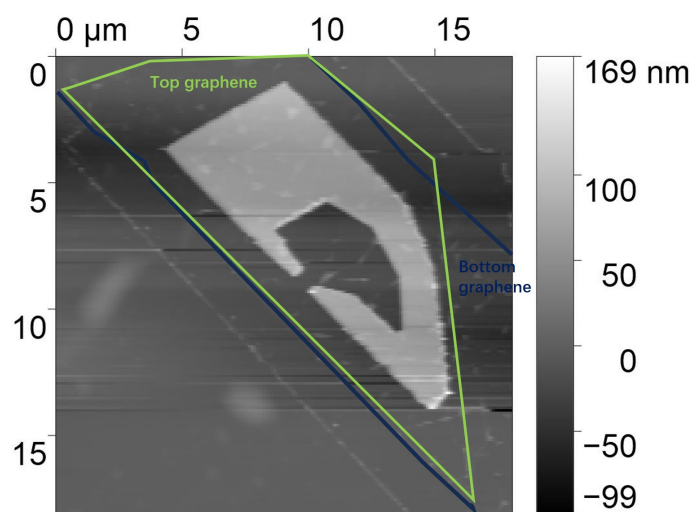


FIG. S4. A tapping-mode AFM image of the rotor device featured in Fig. 3 in the main text. The green line marks the perimeter of the top graphene monolayer attached to the rotor frame.

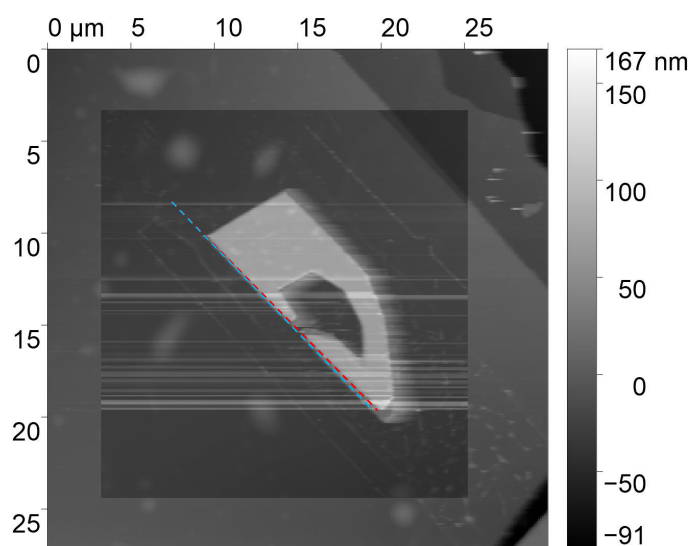


FIG. S5. Superimposed AFM images of the rotor device featured in Fig. 3 prior to manipulation and after the final rotation. The red and blue dotted lines mark the orientations of the same edge before and after the rotation, respectively.



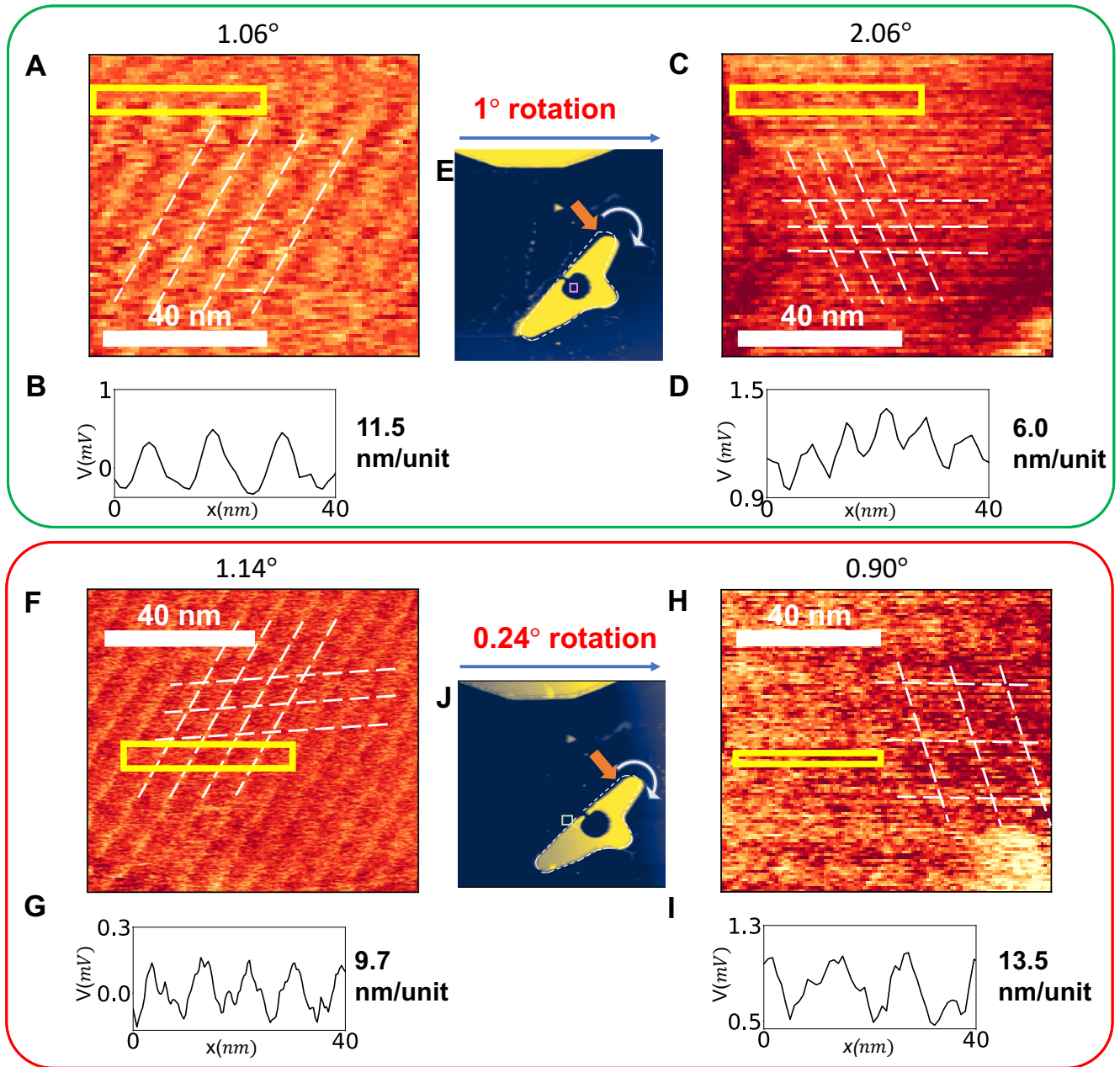


FIG. S6. **Nanoscale control over the period of the moiré superlattice by tip-driven rotations.** (A, C) PFM images of a twisted bilayer graphene rotor device before (A) and after (C) rotation, revealing the change of moiré superlattice period. The twist angle change is  $\Delta\theta = 1^\circ$ . (B, D) 1D line cuts extracted from the PFM images in panels (A) and (C), respectively, showing the change in periodicity of the superlattice induced by the rotation. (E) AFM image of the rotor device, illustrating the tip-induced manipulation responsible for the rotation of the twist angle. The orange arrow represents the location of the AFM tip push, which introduced a displacement of 100 nm. (F, H) PFM images of a twisted bilayer graphene rotor device before (F) and after (H) a separate rotation process, showing the change in the moiré period that is caused by a twist angle change of  $\Delta\theta = -0.24^\circ$ . (G, I) 1D line cuts extracted from the PFM images in panels (F) and (H), respectively, showing the change in periodicity of the superlattice induced by the rotation. (J) The AFM image of the rotor device, illustrating the manipulation responsible for the change in twist angle. The orange arrow represents the location of the AFM tip push, which introduced a displacement of 50 nm.